Chemical vapor deposition of sp^2-boron nitride films on Al_2O_3 (0001), $(11\bar{2}0), (1\bar{1}02)$ and $(10\bar{1}0)$ substrates

Running title: CVD of sp^2-BN on sapphire

Running Authors: Sachin et al.

Sachin Sharma [1, a)] Laurent Souqui [2], Henrik Pedersen[1], Hans Högberg[1]

[1] Department of Physics, Chemistry and Biology (IFM), Linköping University, SE-581 83, Linköping, Sweden.
[2] Department of Materials Science and Engineering, University of Illinois at Urbana-Champaign, 1304 W. Green St, Urbana, Illinois 61801

[a)] Electronic mail: sachin.sharma@liu.se

Thin films of boron nitride in its sp^2-hybridized form (sp^2-BN) have potential use in UV-devices and dielectrics. Here, we explore chemical vapor deposition (CVD) of sp^2-BN on various cuts of sapphire; $Al_2O_3(11\bar{2}0)$, $Al_2O_3(1\bar{1}02)$, $Al_2O_3(1\bar{1}00)$ and Al_2O_3 (0001) using two CVD processes with different boron precursors; triethylborane (TEB) and trimethylborane (TMB). Fourier transform infrared spectroscopy (FTIR) showed that sp^2-BN grows on all the sapphire substrates, using X-ray diffraction (XRD), $2\theta/\omega$ diffractograms showed that only $Al_2O_3(11\bar{2}0)$ and $Al_2O_3(0001)$ renders crystalline films and using phi(ϕ)-scans the growth of rhombohedral polytype (r-BN) films on these substrates is confirmed. These films are found to be epitaxially grown on an AlN interlayer with a higher crystalline quality for the films grown on the $Al_2O_3(11\bar{2}0)$ substrate which is determined using omega(ω)-scans. Our study suggests that $Al_2O_3(11\bar{2}0)$ is the most favorable sapphire substrate to realize the envisioned applications of r-BN films.

I. INTRODUCTION

Epitaxially grown hexagonal and rhombohedral boron nitride (h-BN[1] and r-BN[2]) thin films are materials that have various applications in the fields of UV devices [3–6] and graphene technology[7–10]. Similarly, other less ordered crystalline forms of BN including turbostatic BN (t-BN) and amorphous BN (a-BN) are studied to understand film nucleation, and have potential electronic applications as dielectrics.[11,12] Thin film growth of sp^2-hybridized boron nitride (sp^2-BN) is typically done using chemical vapor deposition (CVD). Growth of epitaxial sp^2-BN thin films requires high growth temperatures, above 1200 °C[13–17], which is a limiting factor for the substrates that can be used. Hitherto, substrates for epitaxially grown h-BN and r-BN phases include 3C-SiC(111), 4H- and 6H-SiC(0001) on-axis substrates and α-Al$_2$O$_3$(0001).[13–15,17,18,19] These substrates resulted in epitaxially grown [0001]-oriented sp^2-BN films where it is challenging to distinguish between h-BN and r-BN phases.[20] Therefore, it is of interest to study epitaxial sp^2-BN films grown in other crystal orientations. Growth of sp^2-BN films on other cuts of sapphire (Al$_2$O$_3$) provides a potential route to explore this possibility. These cuts include Al$_2$O$_3(11\bar{2}0)$, Al$_2$O$_3(1\bar{1}02)$ and Al$_2$O$_3(10\bar{1}0)$ henceforth referred to as *a*-cut, *r*-cut and *m*-cuts respectively, along with the previously investigated Al$_2$O$_3$ (0001) *c*-cut substrates.

We have previously employed an AlN buffer layer to facilitate epitaxial growth of sp^2-BN on *c*-cut sapphire.[13,21] AlN growth on *r*-cut Al$_2$O$_3$ also showed *a*-plane $(11\bar{2}0)$ oriented growth suggesting growth orientations can be altered based on the substrate used.[22] Other studies of AlN growth on *c*-cut and *a*-cut Al$_2$O$_3$ showed that the growth

direction was identical in both cuts of Al_2O_3.[23] This is relevant since the surface nitridation of Al_2O_3 is observed and expected for thermal CVD at such high temperatures. Notably, a recent study on the surface properties of the substrate comparing h-BN growth using diborane (B_2H_6) on *a*-cut and *c*-cut Al_2O_3 revealed the former to be less likely to modify under growth conditions in the absence of an AlN buffer layer.[19] Its noteworthy that when B_2H_6, a carbon free boron precursor, was used, as opposed to trimethylboron (TMB) and triethylboron (TEB), to deposit BN without nitridizing the sapphire, h-BN films are observed.

This study aims to investigate possible growth of sp^2-BN using thermal CVD, comparing the difference of growth on *a*-cut, *r*-cut, *m*-cut and *c*-cut substrates. This growth is done using two different boron precursors TMB and TEB which have been investigated in previous studies.[17,18] Crystalline growth in the polytype r-BN was observed in these studies. The most suitable substrates for specific growth applications will be realized as we identify the major characteristic difference between each substrate.

II. EXPERIMENTAL

A. Film Deposition

The films are deposited using hot wall CVD with two different boron precursors, trimethylboron, $B(CH_3)_3$ (TMB) (99.99% purity, Voltaix/Air Liquide Advance Materials, FL) and triethylboron, $B(C_2H_5)_3$ (TEB) (semiconductor grade quality, from SAFC Hitech). Precursor for nitrogen is ammonia (NH_3, 99.999%, further purified with respect to water using a getter filter) with H_2 (palladium-membrane purified) as the carrier gas.

The boron precursors, in their respective processes, are added through a separate quartz liner along with H_2 to avoid the formation of intermediate adducts prematurely. A pyrometer (Heitronics KT81R, calibrated by a silicon melt test) is used to monitor the growth temperature. The process pressure is maintained using a throttle valve. As observed from prior experience, the addition of silane (SiH_4) has proved useful to promote better crystallinity in the films grown by this process hence added while growing using both precursors.[24]

Optimized processes parameters are selected from previous studies on TEB and TMB.[17,18] For all processes, the base pressure is kept below 2 x 10^{-2} mbar. Carrier gas flow is maintained at 5000 sccm H_2. The growth temperature for the process based on TMB was 1400°C and BN is grown of sp^2-BN 60 min with a process pressure of 50 mbar, while the process based on TEB growth was done at 1500°C and BN is grown for typically 240 min with a process pressure of 70 mbar. The NH_3/TMB ratio was kept at 966. Silane (SiH_4, 99.999 % purity, 2000 ppm diluted in 99.9996 % H_2) was supplied with a flow corresponding to 16.5 sccm 2 minutes prior to BN deposition. The NH_3/TEB ratio was kept at 642. SiH_4 (99.999 % purity, 2000 ppm diluted in 99.9996 % H_2) was supplied with a flow corresponding to 13 sccm 2 minutes prior to film deposition.

All substrates used are sized at 10×10 mm^2 except for the *m*-cut substrates which were 20×20 mm^2. The *c*-cut, *a*-cut, *r*-cut substates are 2", 330 µm-thick on axis substrates manufactured at The Roditi International Corp. Ltd. While the *m*-cut substrate is 2'', 430 µm thick substrate manufactured at MTI Corporation (Materials Tech. Intl.). They are all cleaned with the same procedure which includes 3 minutes in an ultrasonic bath with acetone at 80 °C, 3 minutes in an ultrasonic bath with ethanol at 80 °C, followed by

standard clean 1 (SC1, $NH_3:H_2O_2:H_2O$) with relative concentrations 1:1:26 at 80 °C) and

standard clean 2 (SC2, $NH_3:H_2O_2:H_2O$ with relative concentrations 1:1:22 at 80 °C).[25]

The substrates are then placed in the heating part of the reaction cell(susceptor), this is a

elliptically shaped and this susceptor is coated with tantalum-carbide (TaC). The

depositions on the different substrates are done separately as they are always placed in

the same position in the susceptor for each process. Prior to BN deposition, the α-Al_2O_3

substrates were heated to 1100 °C for 5 min in H_2 gas, after which NH_3 was introduced

and the temperature is ramped to the selected growth temperatures and maintained for 10

min to form an in situ aluminum nitride buffer layer as previously reported.[9,16]

B. Film characterization

Fourier transform infrared spectroscopy (FTIR) reflectance spectra were

measured using a Bruker Vertex70 FTIR spectrometer, with a globar MIR light source

and a DLaTGS detector, the software used here is Bruker OPUS 7.5. The incident s-

polarized light at an angle of 60° with respect to the sample surface normal. The spectra

were acquired at room temperature, after a 30 min N_2 purge, with 2 cm^{-1} resolution and

averaged over 50 scans. A thin film of gold was used as reference. The FTIR peaks were

fitted using a Lorentzian profile and linear base line using SciDAVis software (version

1.22).

X-ray diffraction (XRD) was used to investigate the structural properties and the

crystallographic relationship to the buffer layer and the film orientation. All

diffractograms were recorded using Cu Kα radiation (Cu Kβ removed by a nickel filter).

The 2θ/ω diffractograms were recorded in a PANAlytical X'Pert Pro diffractometer with

a Bragg-Brentano HD and 1/2° slit as primary optics and X'celerator detector with a 5 mm anti scatter slit on the secondary side. The azimuthal scans (ϕ-scans) were recorded in a Phillips X'Pert MPD diffractometer with crossed slits (2×2 mm^2) and 1/2° slit as primary optics and proportional detector (PW1711/96) equipped with parallel plate collimator on the secondary side. Same instrumentation is used to obtain XRD ω-scan (rocking curve) on the crystalline samples. These scans give a measure of the crystal quality of the deposited films. Full width half maximum calculated using PANalytical Data viewer software version 1.3b.

The compositional analysis of the films was performed using time-of-flight energy elastic recoil detection analysis (ToF-ERDA). The measurements are done using a 36 MeV $^{127}I^{+8}$ beam. The incidence angle of primary ions and exit angle of recoils were both 67.5° to the sample surface normal constituting a recoil angle is 45°. The measured ToF-ERDA spectra data is then converted into relative atomic concentration profiles using the Potku code.[26]

The surface morphology of the sp^2-BN films was analyzed using scanning electron microscopy (SEM)1550 Gemini. The microscope was operated with conventional and immersion lens (in-lens) secondary electron detectors and an accelerating voltage of 3 kV.

III. RESULTS AND DISCUSSION

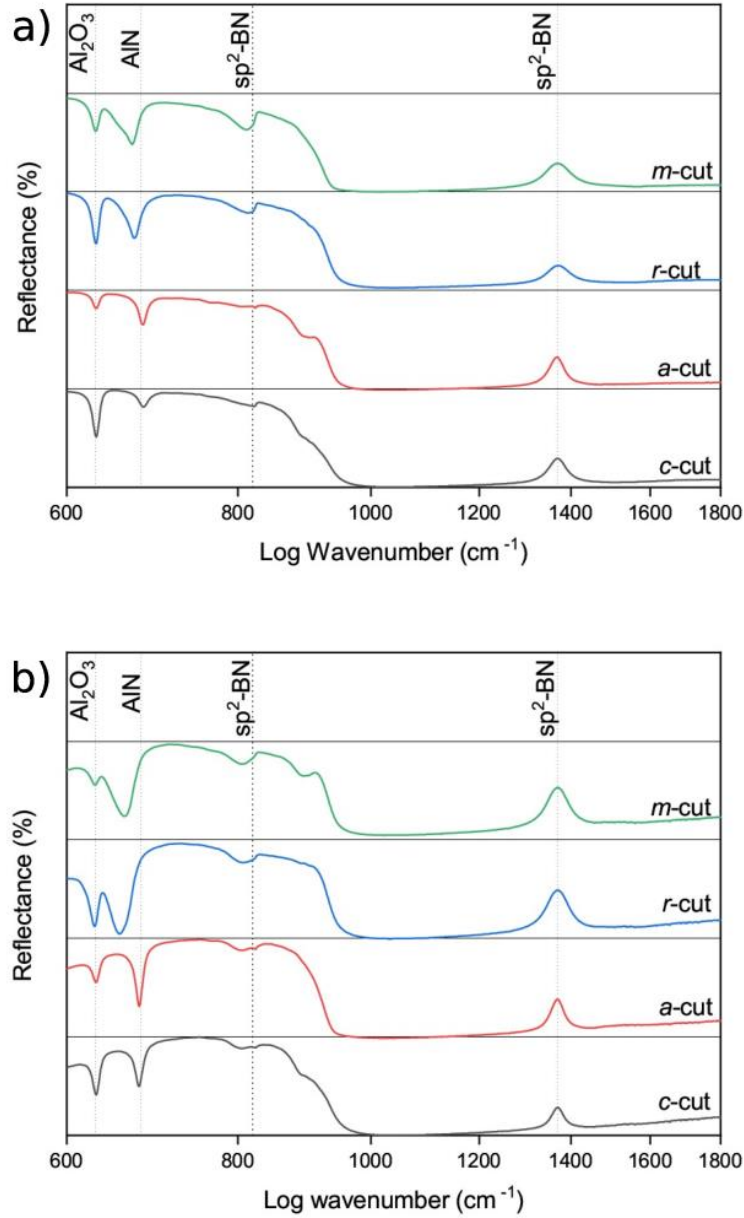## A. *Chemical Bonding States*

Figure 1. (a) FTIR spectra of film growth on all cuts of Al_2O_3 grown using (a) TMB as the boron precursor and (b) using TEB as the boron precursor. Here the substrates used, Al_2O_3 (0001), Al_2O_3 ($11\bar{2}0$), Al_2O_3 ($1\bar{1}02$), Al_2O_3 ($10\bar{1}0$) are called *c*-cut, *a*-cut, *r*-cut and *m*-cut respectively

Figure 1 shows the FTIR transflectance spectrum on all cuts of sapphire after film deposition. Here, transflectance is the sum of reflectance from the film surface and twice the transmittance through the film. For all investigated samples, we observe the transversal optical in-plane mode peaks for sp^2-BN at 1369 cm^{-1}, as well as the longitudinal optical out of plane mode of sp^2-BN at around 820 cm^{-1}.[27] Hence, sp^2-BN films are grown on all studied cuts of sapphire. On these latter bands, sharper absorption bands are observed on the *c*-cut and *a*-cut for both the precursors. These sharp edges are suggested to indicate the crystallinity of these samples.[28] Since, for amorphous material there is a variation in the frequency of the vibrational modes which gives broader peaks compared to crystalline films, suggesting that the sp^2-BN films grown on *r*-cut and *m*-cut sapphire are amorphous.
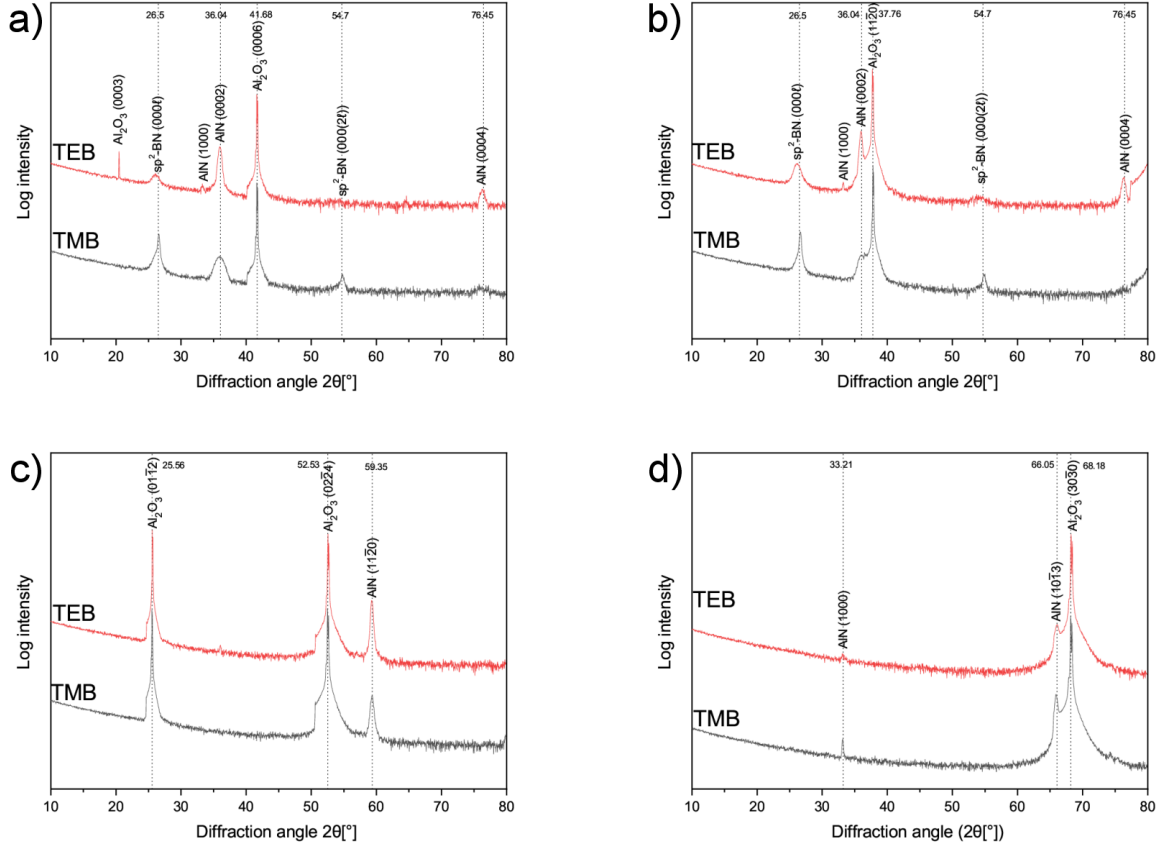
B. Thin Film X-ray Diffraction

Figure 2. 2θ/ω diffraction patterns from BN films deposited on the substrates (a)Al_2O_3 (0001), (b)Al_2O_3 (11$\bar{2}$0), (c) Al_2O_3 (1$\bar{1}$02) and (d) Al_2O_3 (10$\bar{1}$0)

Figure 2(a-d) shows the 2θ/ω diffractogram of the films deposited on different cuts of Al_2O_3 using TEB and TMB. In figures 2(a) and 2(b), for the *c*-cut and *a*-cut substrates show the relatively weaker diffraction peaks around 2θ = 26.5° and 2θ = 55° originate from sp^2-BN (000ℓ) and sp^2-BN (0002ℓ) respectively.[29,30] AlN (0002) and AlN (0004) peaks are observed for both of these samples as well. The hkiℓ here signifies the long-range order in the direction normal to the surface. Samples with TEB as boron precursor have comparatively lower intensities. From previous studies we know that samples grown using the TMB precursor have higher growth rate of sp^2-BN and hence

9

more material is deposited during growth which is reflected in the peak intensity. In figures 2(c) and 2(d) there are no BN peaks, confirming the FTIR results that the BN films present are amorphous on *r*-cut and *m*-cut sapphire. In figure 2(d), i.e. the *r*-cut sample shows AlN $(11\bar{2}0)$ growth, this growth orientation on this substrate has been observed seen in past studies[22,31] and for the *m*-cut samples in fig. 2(d) AlN(1000) and $(10\bar{1}3)$ growth is observed, the latter of which has been reported previously.[32]

Figure. 3. XRD φ-scans of samples 3.(a) on the *c*-cut Al_2O_3 showing the epitaxial relationships between each layer top to bottom r-BN$\{10\bar{1}1\}$ in red (top) measured at ψ = 77.76°, AlN$\{10\bar{1}2\}$ in black (middle) measured at ψ = 61.5°and $Al_2O_3\{11\bar{2}3\}$ in blue (bottom) measured at ψ = 61.2°, 3.(b) on the *a*-cut Al_2O_3 showing the epitaxial relationships between each layer top to bottom r-BN$\{10\bar{1}1\}$ in red (top) measured at ψ =

77.76° and AlN$\{10\bar{1}2\}$ measured at $\psi = 42.75°$as well as Al$_2$O$_3\{01\bar{1}2\}$(marked separately) measured at $\psi = 43°$ in black (bottom). Both samples grown using TMB precursor.

ϕ-scans are used to confirm the epitaxial relationship of the films grown on the c-cut and a-cut Al$_2$O$_3$ using the TMB precursor in figure 3. Here, the in-plane epitaxial relationship can be seen as r-BN$[10\bar{1}0]$ ∥ w-AlN$[10\bar{1}0]$ ∥ α-Al$_2$O$_3[11\bar{2}0]$ on the c-cut Al$_2$O$_3$ and r-BN$[11\bar{2}0]$ ∥ w-AlN$[11\bar{2}0]$ ∥ α-Al$_2$O$_3[0001]$ on the a-cut Al$_2$O$_3$. For both samples there is twinning of the r-BN expected threefold symmetry which is also observed in previous studies, hence 6 peaks are expected.[13,17] Since sp^2-BN diffracts poorly, longer scan times were used for these ϕ-scans which is why a background subtraction and signal smoothening is applied. The low intensity for a few peaks observed is due to the high tilt sensitivity of the sample at higher ϕ angles. Twinning of AlN grown on c-cut Al$_2$O$_3$ is observed.[33]

XRD ω-scans on the films grown using TMB provide crystal properties and shows the difference in crystalline quality of the films grown. The a-cut sample shows lower FWHM of 0.985° compared to 1.155° of the c-cut sample which is a difference of about 15%. Further confirming suggestions of a more suitable substrate in a-cut Al$_2$O$_3$ for the growth of sp^2-BN.[19] Small deviation from the expected ω peak angle suggests very slight buckling in the film surface with respect to the substrate. Broadness of the peaks suggest a less ordered film with respect to the substrate. Samples grown using TMB are compared in the ϕ-scans and ω-scans due to the difference in amount of sp^2-BN present as described above.
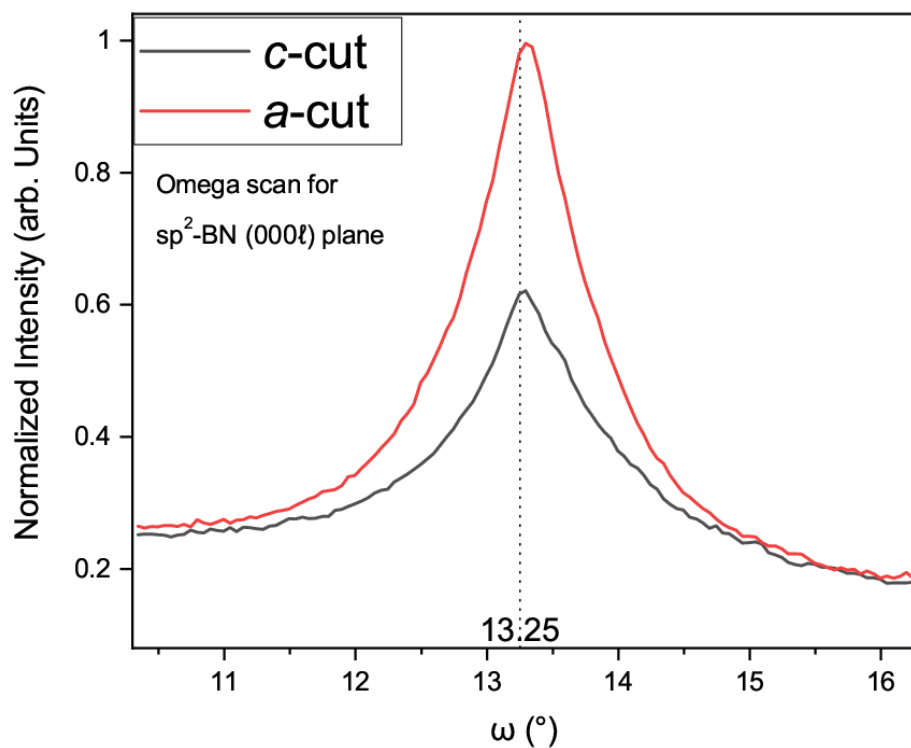
Figure. 4. XRD ω-scans of the crystalline films grown on *c*-cut and *a*-cut Al$_2$O$_3$ using the TMB precursor. Dotted line corresponds to the ω-angle which is half of the 2θ-angle for the sp^2-BN (000ℓ) peak at 26.5
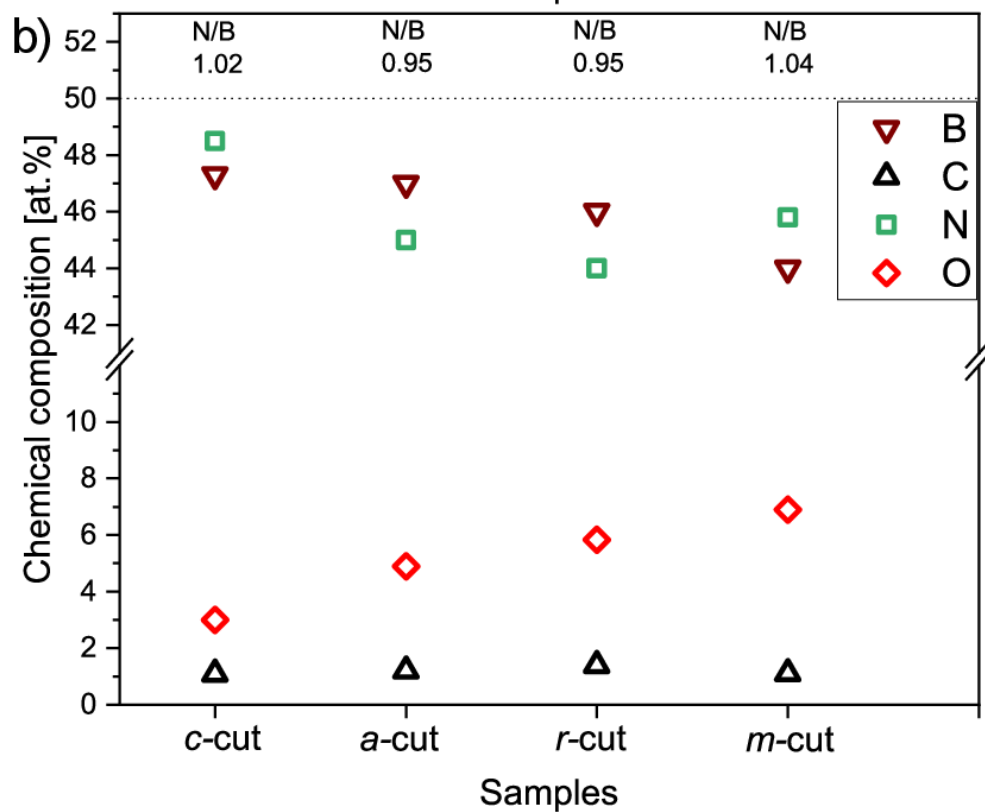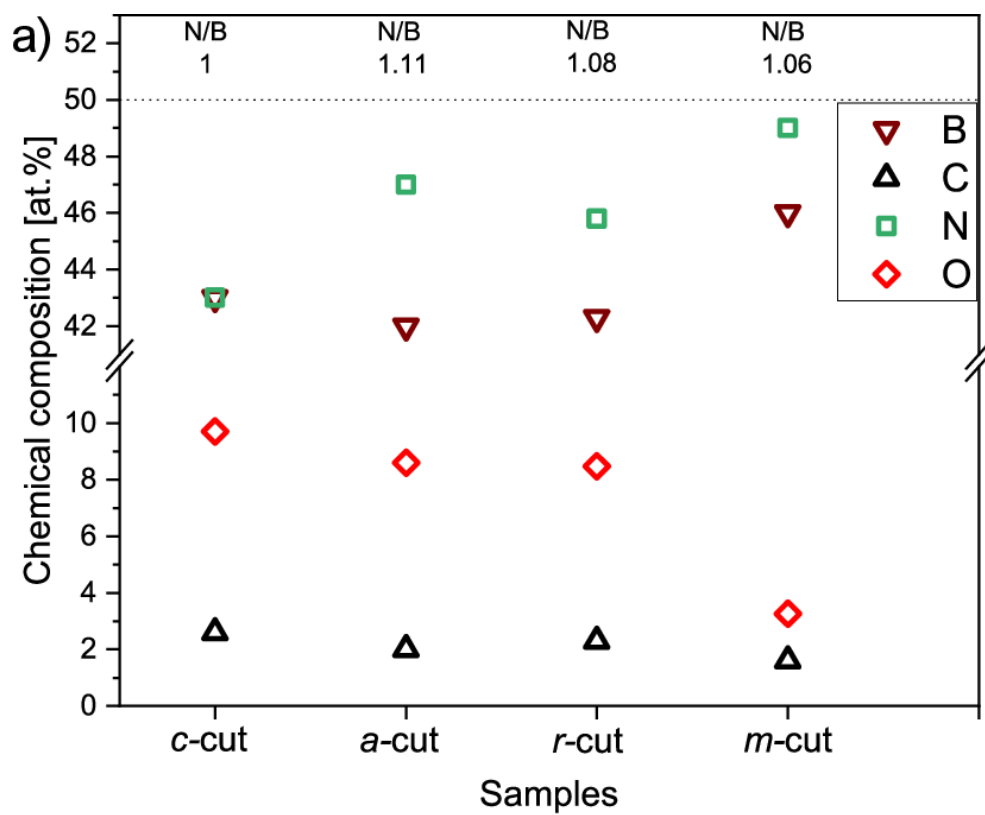
C.   Elemental Composition

Figure 5. ToF-ERDA analysis is used to calculate the elemental compositions of the samples, (a) Samples grown using TMB precursor (b) Samples grown using TEB precursor. Here the substrates used, Al_2O_3 (0001), Al_2O_3 ($11\bar{2}0$), Al_2O_3 ($1\bar{1}02$), Al_2O_3 ($10\bar{1}0$) are called c-cut, a-cut, r-cut and m-cut respectively

As observed from the ToF-ERDA results in figures 5(a) and 5(b), the samples grown using TEB as the boron precursor show more consistent stoichiometry and a better nitrogen to boron (N/B) ratio compared to the TMB grown samples. For the TEB samples, growth on the c-cut substrates display the least amount of oxygen contamination. Samples grown using TMB as the boron precursor display varying quantities of oxygen in the films, at this stage it is assumed to be a function of the difference in the amount grain boundaries on the films, which leads to oxidation post deposition. The m-cut sample grown using the TMB precursor displays film growth with least amounts of oxygen which could potentially be due to the denser amorphous microstructure on this cut. Looking at the film surface structure would provide further insight (Fig. 6). Hydrogen content is very low (<0.2%) and thus omitted. Overall, lower quantities of C and higher quantities of B is seen on the film grown using TEB compared to TMB which agrees with results from past studies.[34]
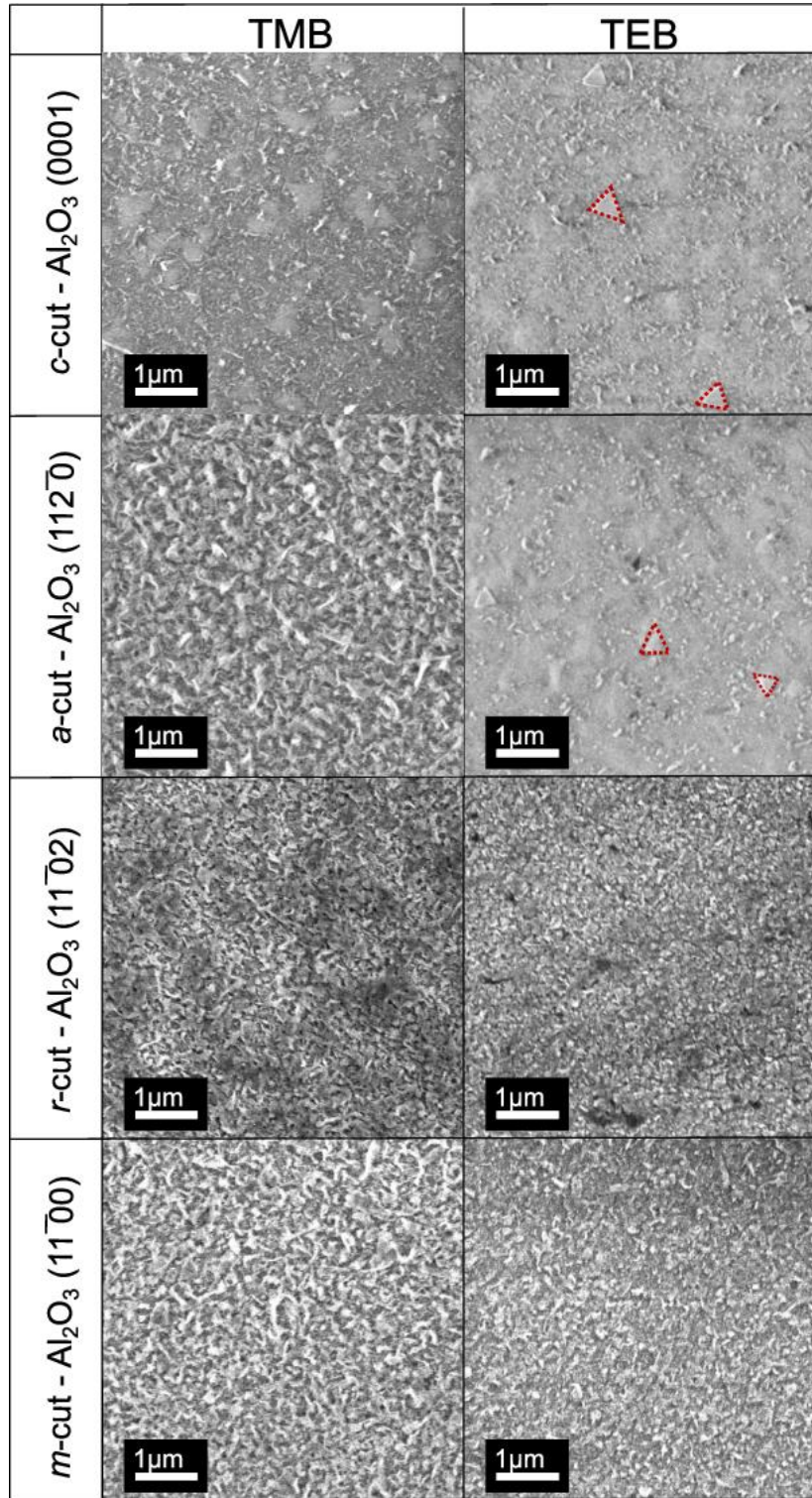
15

D.   Surface Morphology

Figure 6. Plan-view SEM micrographs of film growth on all cuts of Al_2O_3 (top to bottom) grown using TMB (left column) and TEB (right column) as the boron precursor.

Plan-view SEM micrographs reveal that for the substrates that showed r-BN growth, being the c-cut and a-cut Al_2O_3 grown using TEB precursor, forms films with previously observed triangular shaped grains of comparable sizes surrounded by a less ordered material with substantial whisker growth.[21] For the samples grown using TMB, the c-cut sample show similar crystal islands but not shaped as consistently as when deposited from TEB. On the a-cut sample, there are no ordered crystals observed on the plan-view, which could be attributed to deposition of disordered material on the topmost layers. The plan-view SEM of sp^2-BN grown films on the r-cut and m-cut Al_2O_3 is consistent with the expected amorphous film structure suggested in the XRD (Fig.2) and FTIR (Fig.1) results.

E.   Crystallinity

From XRD results on specifically the c-cut and a-cut Al_2O_3, we can conclude that the out of plane crystalline growth direction for r-BN is still identical, being sp^2-BN (000ℓ) and sp^2-BN (000$\underline{2}\ell$), between the two substrates. These substrates also show identical AlN 0002 and AlN 0004 peaks, this result was also observed in a past study on AlN growth on these Al_2O_3 substrates.[23] The potential for a new growth direction was not realized, but a-cut Al_2O_3 showed comparable crystal properties to the c-cut with better crystalline quality as supported by the ω-scan (Fig. 4) for the growth of r-BN films. These results agree with suggestions from a recent surface study of BN growth on a-cut Al_2O_3, which described it to be more suitable for the growth of h-BN.[19] The presence of AlN 0002 and AlN 0004 peaks on both c-cut and a-cut Al_2O_3 evidently dictates the epitaxial r-BN film growth on these substrates. Supported by previous studies that have shown that h-BN initially nucleates epitaxially followed by r-BN epitaxial film growth on AlN (0001) grown on c-cut sapphire.[35] In contrast, for r-cut and m-cut Al_2O_3 we don't detect AlN 0002 and AlN 0004 peaks, instead we observe AlN ($11\bar{2}0$) and mostly AlN ($10\bar{1}3$) growth on these cuts respectively. Since the crystal direction of the AlN film

17

dictates the growth direction of the r-BN film, we would expect growth of crystalline BN films on these substrates. Instead, a-BN growth is observed on *r*-cut and *m*-cut substrates. We speculate that this could be explained due to the higher surface energies of the off-axis BN planes preventing crystalline BN film growth for these substrates.

IV. CONCLUSIONS

We report the differences in CVD growth of sp^2-BN films with TMB and TEB on different Al_2O_3 substrates ($Al_2O_3(11\bar{2}0)$, $Al_2O_3(1\bar{1}02)$, $Al_2O_3(10\bar{1}0)$ and Al_2O_3 (0001) called *a*-cut, *r*-cut, *m*-cut and *c*-cut respectively). FTIR shows the presence of sp^2-BN films on each substrate, but XRD shows crystalline sp^2-BN only on the *c*-cut and *a*-cut substrates. Epitaxial growth of the polytype r-BN is confirmed with the in-plane relationships r-BN[$10\bar{1}0$] ∥ w-AlN[$10\bar{1}0$] ∥ α-Al$_2$O$_3$[$11\bar{2}0$] on the *c*-cut Al$_2$O$_3$ and r-BN[$11\bar{2}0$] ∥ w-AlN[$11\bar{2}0$] ∥ α-Al$_2$O$_3$[0001] on the *a*-cut Al$_2$O$_3$. Our studies show that *a*-cut Al$_2$O$_3$ should be considered as a viable substrate for crystalline growth of r-BN polytype displaying better crystalline quality even compared to commonly used *c*-cut. This result is promising towards improving crystal quality of r-BN for envisioned applications and studies in the future.

DATA AVAILABILITY

The data that support the findings of this study are available within the article.

REFERENCES

[1] R.S. Pease, Acta Crystallogr. **5**, 356 (1952).

[2] D. Golberg, Y. Bando, L. Bourgeois, K. Kurashima, and T. Sato, Appl. Phys. Lett. **77**, 1979 (2000).

[3] K. Watanabe, T. Taniguchi, and H. Kanda, Nat. Mater. **3**, 404 (2004).

[4] K. Ahmed, R. Dahal, A. Weltz, J.Q. Lu, Y. Danon, and I.B. Bhat, Appl. Phys. Lett. **109**, (2016).

[5] Y. Kubota, K. Watanabe, O. Tsuda, and T. Taniguchi, Science (80-.). **317**, 932 (2007).

[6] H. Liu, J. Meng, X. Zhang, Y. Chen, Z. Yin, D. Wang, Y. Wang, J. You, M. Gao, and P. Jin, Nanoscale **10**, 5559 (2018).

[7] M. Yankowitz, J. Xue, and B.J. Leroy, J. Phys. Condens. Matter **26**, (2014).

[8] R.Y. Tay, S.H. Tsang, M. Loeblein, W.L. Chow, G.C. Loh, J.W. Toh, S.L. Ang, and E.H.T. Teo, Appl. Phys. Lett. **106**, (2015).

[9] S. Nakhaie, J.M. Wofford, T. Schumann, U. Jahn, M. Ramsteiner, M. Hanke, J.M.J. Lopes, and H. Riechert, Appl. Phys. Lett. **106**, (2015).

[10] W. Gannett, W. Regan, K. Watanabe, T. Taniguchi, M.F. Crommie, and A. Zettl, Appl. Phys. Lett. **98**, 242105 (2011).

[11] X.T. Zhou, T.K. Sham, C.Y. Chan, W.J. Zhang, I. Bello, S.T. Lee, F. Heigl, A. Jürgenen, and H. Hofsäss, J. Mater. Res. **21**, 147 (2006).

[12] Q. Abbas, H. Liang, J. Shi, Y. Chen, X. Xia, A. ul Ahmad, J. Liu, and G. Du, Mater. Lett. **227**, 284 (2018).

[13] M. Chubarov, H. Pedersen, H. Högberg, J. Jensen, and A. Henry, Cryst. Growth Des. **12**, 3215 (2012).

[14] N. Umehara, A. Masuda, T. Shimizu, I. Kuwahara, T. Kouno, H. Kominami, and K. Hara, in *Jpn. J. Appl. Phys.* (Japan Society of Applied Physics, 2016).

[15] M. Chubarov, H. Pedersen, H. Högberg, Z. Czigany, and A. Henry, CrystEngComm **16**, 5430 (2014).

[16] M. Chubarov, H. Pedersen, H. Högberg, V. Darakchieva, J. Jensen, P.O.Å. Persson, and A. Henry, Phys. Status Solidi - Rapid Res. Lett. **5**, 397 (2011).

[17] L. Souqui, H. Pedersen, and H. Högberg, J. Vac. Sci. Technol. A **37**, 020603 (2019).

[18] L. Souqui, J. Palisaitis, N. Ghafoor, H. Pedersen, and H. Högberg, J. Vac. Sci. Technol. A **39**, 013405 (2021).

[19] A. Bansal, M. Hilse, B. Huet, K. Wang, A. Kozhakhmetov, J.H. Kim, S. Bachu, N. Alem, R. Collazo, J.A. Robinson, R. Engel-Herbert, and J.M. Redwing, ACS Appl. Mater. Interfaces (2021).

[20] M. Chubarov, H. Pedersen, H. Hogberg, S. Filippov, J. Engelbrecht, J. O'Connel, and A. Henry, in *Pacific Rim Conf. Lasers Electro-Optics, CLEO - Tech. Dig.* (2013).

[21] M. Chubarov, H. Pedersen, H. Högberg, A. Henry, and Z. Czigány, J. Vac. Sci. Technol. A Vacuum, Surfaces, Film. **33**, 061520 (2015).

[22] C.H. Lin, D. Yasui, S. Tamaki, H. Miyake, and K. Hiramatsu, Jpn. J. Appl. Phys. **55**, (2016).

[23] H. Fukuyama, S.Y. Kusunoki, A. Hakomori, and K. Hiraga, J. Appl. Phys. **100**, (2006).

[24] M. Chubarov, H. Pedersen, H. Högberg, and A. Henry, CrystEngComm **15**, 455 (2013).

[25] W. Kern, *The Evolution of Silicon Wafer Cleaning Technology* (n.d.).

[26] K. Arstila, J. Julin, M.I. Laitinen, J. Aalto, T. Konu, S. Kärkkäinen, S. Rahkonen, M. Raunio, J. Itkonen, J.P. Santanen, T. Tuovinen, and T. Sajavaara, Nucl. Instruments Methods Phys. Res. Sect. B Beam Interact. with Mater. Atoms **331**, 34 (2014).

[27] R. Geick, C.H. Perry, and G. Rupprecht, Phys. Rev. **146**, 543 (1966).

[28] R.L. Hudson and E.F. Mullikin, Spectrochim. Acta - Part A Mol. Biomol. Spectrosc. **207**, 216 (2019).

[29] T. Sato, Proc. Japan Acad. Ser. B Phys. Biol. Sci. **61**, 459 (1985).

[30] D. Belforti, S. Blum, and B. Bovarnick, Nature **190**, 901 (1961).

[31] M. Jo and H. Hirayama, Jpn. J. Appl. Phys. **55**, 5 (2016).

[32] X. Li, J. Zhao, T. Liu, Y. Lu, and J. Zhang, Materials (Basel). **14**, 1722 (2021).

[33] T. Liu, J. Zhang, X. Su, J. Huang, J. Wang, and K. Xu, Sci. Rep. **6**, 1 (2016).

[34] M. Imam, L. Souqui, J. Herritsch, A. Stegmüller, C. Höglund, S. Schmidt, R. Hall-Wilton, H. Högberg, J. Birch, R. Tonner, and H. Pedersen, J. Phys. Chem. C **121**, 26465 (2017).

[35] M. Chubarov, H. Pedersen, H. Högberg, Z. Czigány, M. Garbrecht, and A. Henry, Chem. Mater. **27**, 1640 (2015).